Article:

The effect of molybdenum on interphase precipitation and microstructures in microalloyed steels containing titanium and vanadium

P. Gong[1], X.G. Liu[1], A Rijkenberg[2], W.M. Rainforth[1]*

[1]Department of Materials Science and Engineering, The University of Sheffield, Sir Robert Hadfield Building, Mappin Street, Sheffield, S1 3JD, UK
[2]Tata Steel, 1970 CA IJmuiden, The Netherlands
3National Key Laboratory of Science and Technology on Vacuum Technology and Physics, Lanzhou Institute of Physics, Lanzhou, Gansu, 730010, China

Abstract

Despite much research into steels strengthened through interphase precitation, there remains much that is not clear, such as the role of a range of elements, particularly Mo, in the interphase precipitation process. Four steels were manufactured with identical composition, but with variations in Ti, V, Mo and N content to investigate the effect of composition on interphase precipitation. Alloys were rapidly cooled from the single austenite phase field and isothermally transformed at 630°C and 650°C for 90min. The addition of Mo was found to significantly reduce the austenite to ferrite transformation kinetics, particularly for the V steel. Interphase precipitation was observed in all alloys at both transformation temperatures. For the Ti bearing steel, the two types of precipitate were observed throughout the sample, namely TiC (finer) and Ti_2C (coarser), while for the V bearing steels, VC (finer) and V_4C_3 (coarser) were observed. Where Mo was present in the alloy, it was found dissolved in all carbide types. The (Ti,Mo)C and (V,Mo)C formed by classical planer interphase precipitation (PIP) while the $(Ti,Mo)_2C$ and $(V,Mo)_4C_3$, that had a much wider row spacing, formed through curved interphase precipitation (CIP). Each adopted one variant of the Baker-Nutting orientation relationship. The Ti-microalloyed steels exhibited the smallest precipitates of all the steels, which were approximately the same size irrespective of whether Mo was present in the alloy and irrespective of the transformation temperature. However, the addition of Mo to the V bearing steels resulted in a significant increase in precipitate volume fraction and a reduction in precipitate size. The mechanisms of interphase precipitation leading to the coincident production of two different precipitate types is considered and the role of Mo on the interphase precipitation process is discussed. The resultant effect on strength is considered.

Keywords: Microalloyed steels; interphase precipitation; molybdenum, dilatometry.

*Corresponding author: m.rainforth@sheffield.ac.uk

1. Introduction

Mannerkoski [1] and Relander [2] were the first researchers to investigate interphase precipitation during the austenite to ferrite transformation in alloy steels. Honeycombe and co-workers [3] proposed two distinguishable modes for forming alloy carbides: interphase precipitation and the formation of fibrous carbides during isothermal heat treatment. Interphase precipitation was believed to be nucleated at the immobile semicoherent terraces of the austenite/ferrite interface and delineate the prior positions of the austenite/ferrite interface [4,5]. Further analysis indicated that the morphologies of interphase precipitate carbides could be separated into three types: planar interphase precipitation with regular sheet spacing (PIP); curved interphase precipitation with regular sheet spacing (CIP); and curved interphase precipitation with irregular sheet spacing (irregular CIP) [4,6,7]. Extensive research has been focused on the formation mechanisms of the different types of interphase precipitation [8-13]. For example, earlier work by Davenport and Honeycombe [14] revealed that the interphase precipitates could form on the lowest-energy planar dislocation boundary during the growth of the ferrite through the ledge mechanism. However, this theory has been superseded by the austenite/ferrite phase transformation theories, including the ledge mechanism associated with PIP; the bowing mechanism for irregular CIP and the quasi-ledge mechanism for CIP precipitation [15]. Although the precipitate row spacing is regular, the precipitate spacing within an individual row is randomly distributed [7,10,16-19].

Nb, Ti, Mo and V are well known microalloy additions that refine the grain size, retard recrystallization and provide fine carbide or carbo-nitride precipitates, all of which lead to improved mechanical properties [20-27]. However, such additions also influence the kinetics of the austenite to ferrite transformation and therefore influence interphase precipitation.

2

Additions of Ti, V and Nb increase the transformation kinetics, while additions of Cr, Mo and W have the opposite effect and slow down the transformation [28]. It has been reported that Mo can retarded interphase precipitation during isothermal heat treatment, via the classical interphase precipitation mechanism [8,10,12,13,16,17,29-33]. Early results focused on the study of the physical and chemical properties of transition metal carbides such as (M,Mo)C, where M is Nb, V, Ti [5,18,19,27,34]. However, little research has focused on the effect of Mo on the final microstructure in terms of ferrite grain size and precipitate size and volume fraction and thereby final mechanical properties. Moreover, it is not entirely clear what role Mo plays on the interfacial velocity and the misfit and interfacial energy of the interphase precipitation with the ferrite matrix.

In order to systematically understand these effects, four steels were prepared with the same base-line composition (C, Mn, Si). Two of these steels were based on Ti microalloy additions, one free from Mo, the other with a Mo addition. The remaining three steels were based on a V microalloy addition, one with V only and one with V and Mo. Following austenetisation, rapid cooling was undertaken to the isothermal transformation temperature (which would simulate the coiling temperature after hot rolling). Two temperatures were chosen on the basis of past investigations of the effect of coiling temperature on microstructure (which was part of a programme to develop a commercial advanced strength steel based on precipitation strengthened ferritic structure). Detailed analysis of the interphase precipitates has been undertaken, with a particular focus on precipitate structure, its size and volume fraction and its orientation relationship with the ferrite matrix in order to understand the role that Mo takes in the Ti and V microalloyed steels.

2. Experimental Procedure

2.1. Material

The chemical composition of four laboratory cast microalloyed steels used in the research containing Ti (N1), Ti+Mo (N2), V (N3) and V+Mo (N4), which are listed in Table 1. The alloys were made by vacuum induction melting and cast into ingots having dimensions 620mm × 105mm × 35mm at Tata Steel, IJmuiden. The ingots were homogenized at 1250°C for 2h and hot worked in several passes to 8mm thick plates. The dilatometer specimens, 120mm long × 12mm wide × 6mm thick, were machined from the plate along the rolling direction. The heat treatment for producing interphase precipitated carbides was performed using the Dilatronic dilatometer at The University of Sheffield. Samples were reheated to 1250°C, held for 30min in a tube furnace, and then water cooled to the room temperature. The specimens were then austenitized at 1200°C for 3min and cooled to 630°C and 650°C at a rate of $10°C/s^{-1}$, held isothermally for 90min, and finally water quenched to room temperature. The heat treatment schedule is illustrated in Fig. 1.

Table 1
Chemical composition of the experimental steels (wt%)

| Martials	C	Si	Mn	Al	V	Ti	N	Mo
N1	0.1	0.2	1.6	0.045	-	0.2	≤10ppm	-
N2	0.1	0.2	1.6	0.045	-	0.2	≤10ppm	0.5
N3	0.1	0.2	1.6	0.045	0.2	-	≤10ppm	-
N4	0.1	0.2	1.6	0.045	0.2	-	≤10ppm	0.5
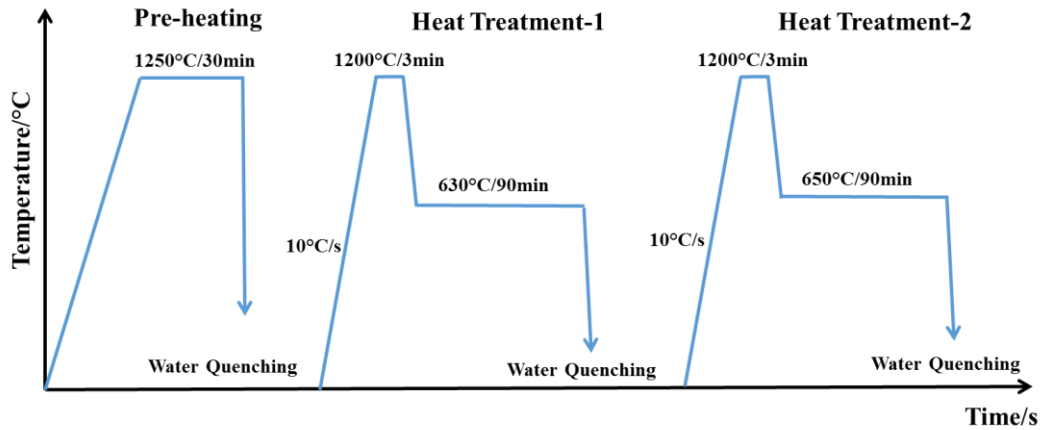
Fig. 1. Schematic of the thermomechanical cycles used and nomenclature used for each condition.

2.2. Grain size and microhardness

The dilatometer specimens were prepared for metallographic examination using standard techniques and then etched in 2% nital solution for approximately 5-10s. The ferrite grain size was measured using the linear intercept method (ASTM E-112) by optical microscopy (OM) and the volume fraction of ferrite in the optical specimens were determined by point counting method via Image J software. Microhardness testing was conducted using a Durascan 70 micro-hardness tester on the polished ferrite grains in the optical samples. A Vickers diamond indenter tip was used with load of 0.5N and a hold time of 15s for each micro-hardness tests. An array of micro-hardness tests were performed at distances of 0.5mm with thirty test measurements on each sample. A small load of 0.5N was chosen to ensure the measurement was taken from the ferrite grains alone, without the influence of neighboring martensite (which formed from the austenite that remained at the end of the isothermal hold, during subsequent rapid cooling).

2.3. Precipitate analysis

Transmission electron microscopy (TEM) was carried out to identify the interphase precipitation from dilatometer specimens. Carbon extraction replicas were used to measure precipitate size and composition. The size distribution from carbon replicas was compared to

that from STEM images from thin foil samples and was found to be the same within experimental error. Thin foils were used to determine precipitate distribution, orientation relationship and confirm precipitate size. Carbon extraction replicas were prepared in the standard manner using a light 2% nital etch. Thin foils for TEM were electropolished using an electrolyte solution of 5% perchloric acid, 35% butoxyethanol and 60% methanol. Extraction replica samples and thin foil samples were examined using an FEI Tecnai T20 and JEOL 2010F TEM, both operated at 200kV. The particle diameter distribution of precipitates was measured for each sample, with around 200 particles counted in each case, with quantitative image analysis being performed using Image J software. The measurement of the sample thickness was also carried out using EELS. This was estimated from the low energy region of the spectrum, given by Eq. (1) [35,36]:

$$t = \lambda ln(I_t/I_0) \tag{1}$$

where t represents the thickness of material; λ is the mean free path of specimen; I_t is the total number of electrons in the EEL spectrum and I_0 is the number of electrons in the zero loss peak.

3. Results

3.1 Microstructure

All optical micrographs were taken from the dilatometer specimens with isothermal heat treatment at 630°C and 650°C for 90min. The microstructure, Fig. 2, mainly comprised polygonal ferrite, formed during isothermal transformation. The volume fraction of ferrite in the Ti-microalloy steels was higher than in the V-microalloy steels. In addition, martensite was present, which formed from the untransformed austenite on cooling at the end of the isothermal hold. Fig. 3 shows the average ferrite grain size, which was measured from optical micrograph images presented in Fig. 2.

The average ferrite grain size for the Ti-microalloyed steels (N1 and N2) was smaller than that of N3 and N4 of V-microalloyed steels at both 630°C and 650°C temperatures. The grain size was slightly larger after transformation at 650°C than at 630°C for the same holding time for all steels. The effect of transformation temperature on grain size was most marked for the Ti microalloyed steels, less so for the V microalloyed steels. For the same composition, the addition of Mo gave a small reduction in grain size (compare N1 with N2 and N3 with N4), the grain size were similar or slightly less than that in the N1 or N3 steels respectively.
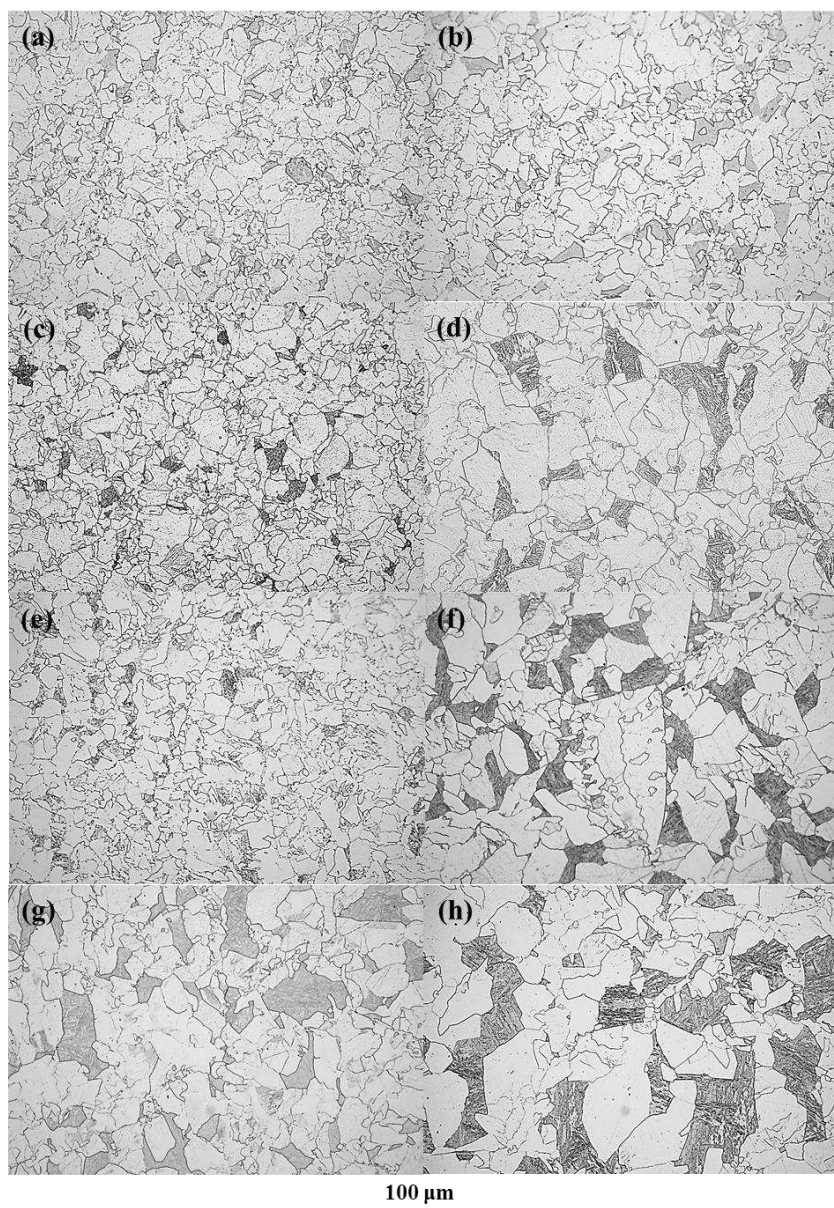

Fig. 2. Optical micrographs taken from specimens isothermally treated at 630°C for 90min on (a) N1; (c) N2; (e) N3; (g) N4; and at 650°C for 90min on (b) N1; (d) N2; (f) N3; (h) N4.
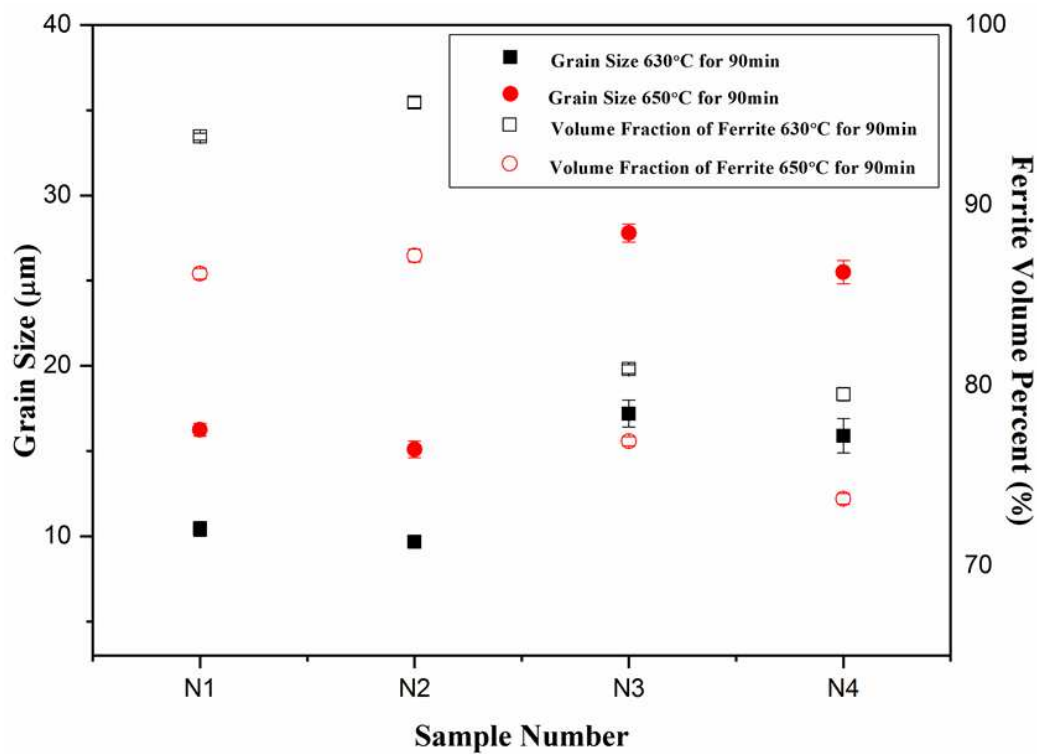
Fig. 3. Variation of ferrite grain size and ferrite volume fraction for the various steels transformed at 630°C and 650°C for 90min.

3.2 Kinetics of the phase transformation

Fig. 4 shows the dilatation curves of the four steels, isothermally transformed at 630°C and 650°C for 90min. For both transformation temperatures and both steels the addition of Mo reduced the rate of transformation (compare N1 with N2 and N3 with N4). The transformation was generally faster at 650°C compared to 630°C for all steels except N2. The reduction in transformation kinetics by the Mo addition was much more evident for the V-microalloyed steel than for the Ti-microalloyed steel at both temperatures, so, Mo had a greater effect on the phase transformation in the V-microalloys steels than in the Ti-microalloy steels.
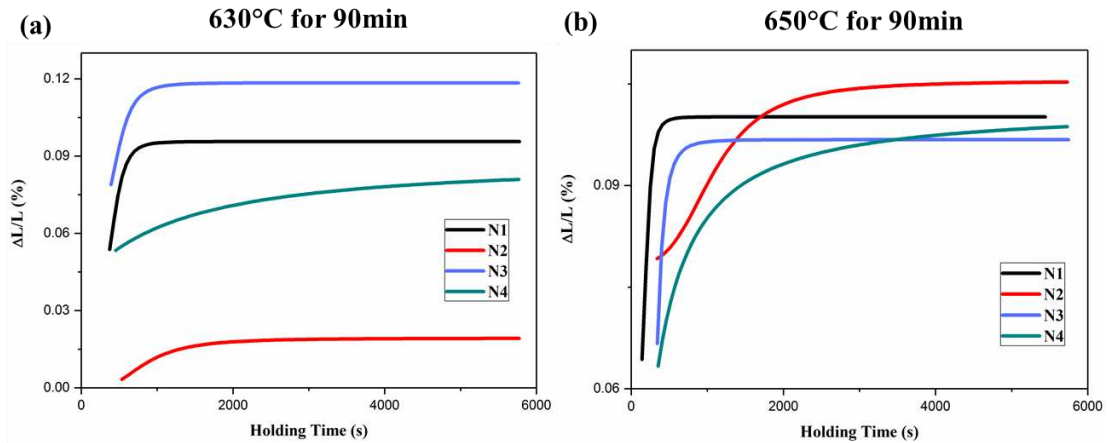
Fig. 4. Dilatation curves of the specimens isothermally treatment at (a) 630°C for 90min; (b) 650°C for 90min.

3.3 Transmission electron microscopy of the interphase precipitation

3.3.1. Precipitate size distribution

To understand the morphology, size and volume fraction of the precipitates in the four steels, TEM was undertaken. The size of precipitates measured from carbon extraction replica samples is shown in Fig. 5. The size and morphology of precipitates differed from steel to steel and also as a function of the transformation temperature. A size distribution analysis is presented in Fig. 6, while the average size, volume fraction and number density of the precipitates is presented in Fig. 7. The precipitate size distribution was found to be the same, within experimental error, for extraction replica and thin foil samples. For the Ti microalloyed steels, the average radius of the precipitates did not measurably change with transformation temperature or with the addition of Mo. The average precipitate radius in the V-microalloyed steels was larger than that in the Ti-microalloyed steels for all compositions. The addition of Mo significantly reduced the precipitate radius by around 2nm for both transformation temperatures.

9
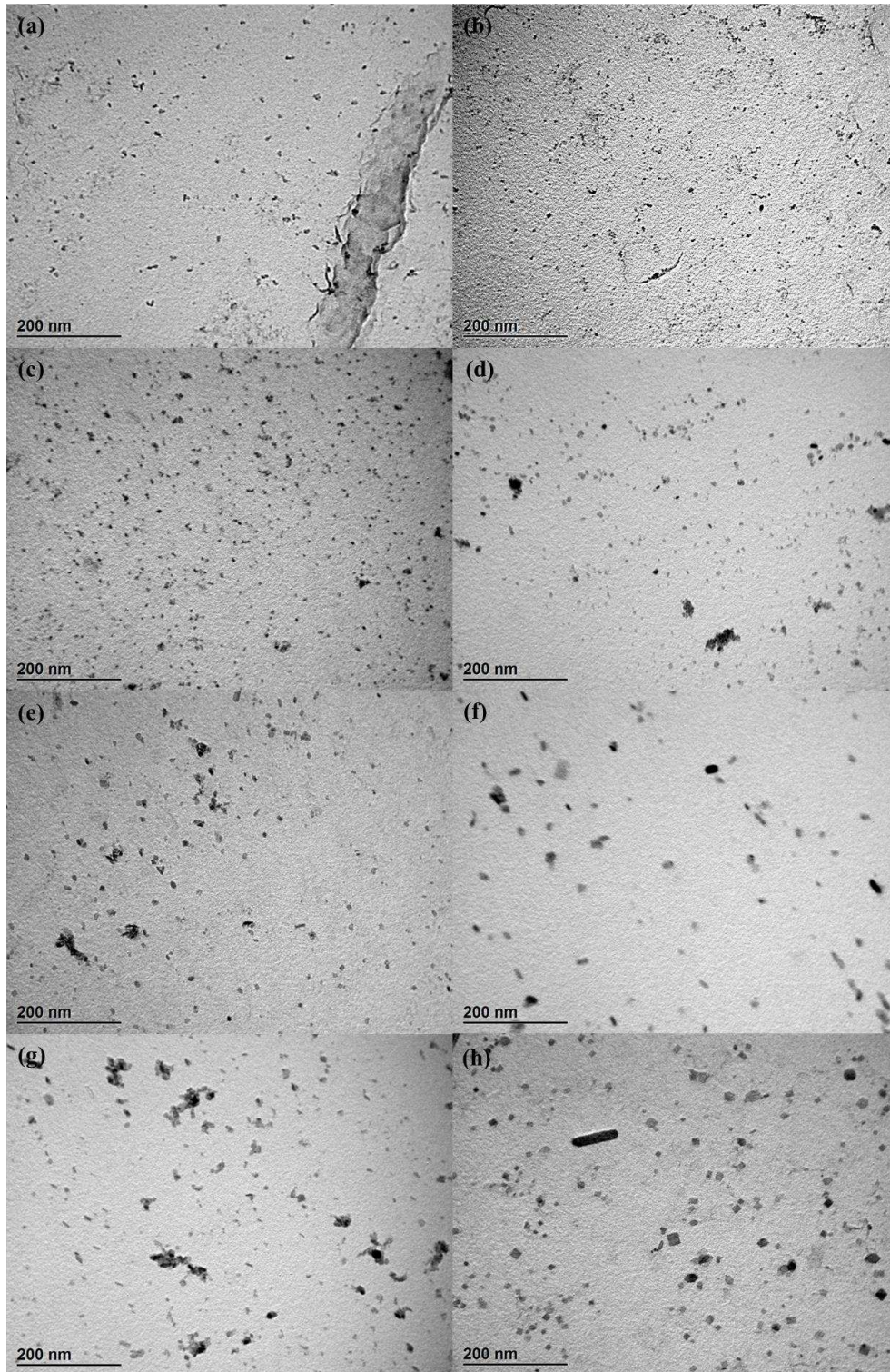
Fig. 5. TEM observation of interphase precipitation from replica samples in different composition of steels taken from specimens isothermally treated at 630°C for 90min on (a) N1; (c) N2; (e) N3; (g) N4; and at 650°C for 90min on (b) N1; (d) N2; (f) N3; (h) N4.
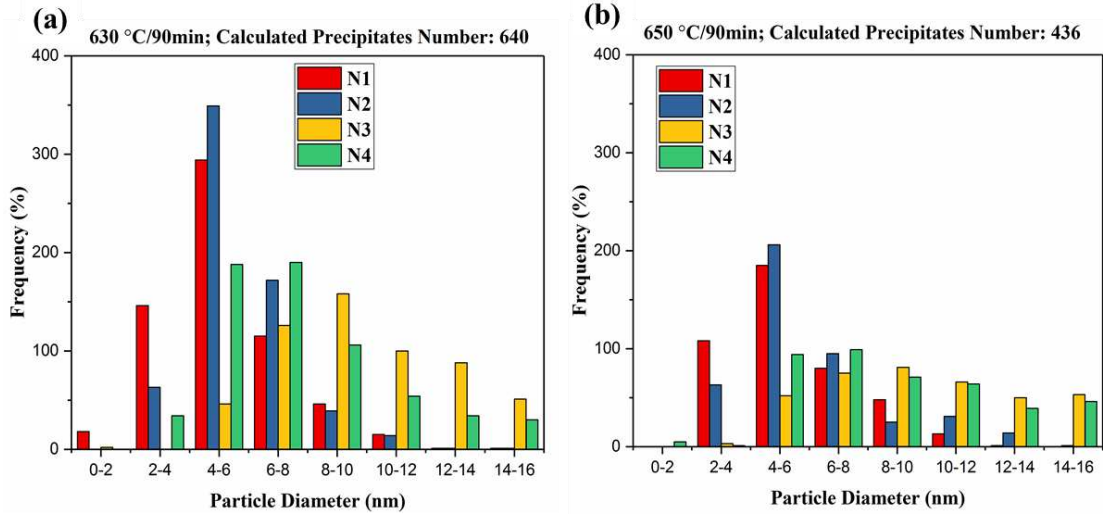
Fig. 6. Size distributions of the precipitates from all samples at the two transformation tempertures: (a) at 630°C for 90min; (b) at 650°C for 90min.
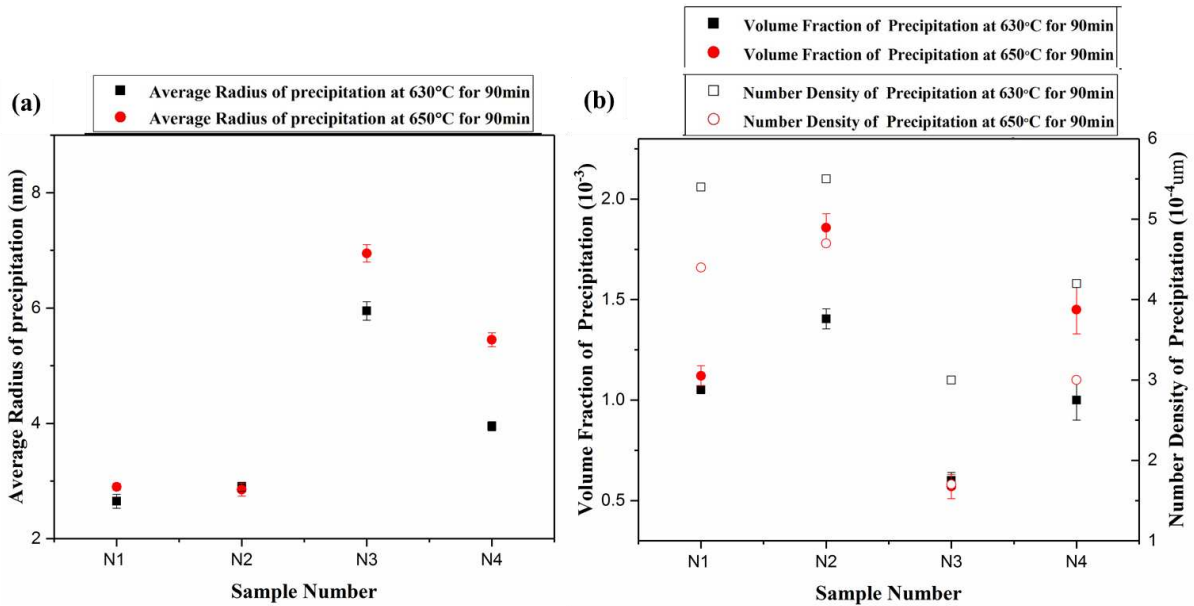
Fig. 7. The volume fraction, average radius size of precipitation and number density of the precipitates in the different steels, isothermally treated at 630°C and 650°C for 90min: (a) average radiums of precipitates; (b) the volume fraction and the number density of precipitates.

By taking into account the thickness of the extraction replica (from EELS zero loss measurements), the volume fraction of the precipitates was measured. Large precipitates (>20nm) were removed from the data as they do not contribute to strengthening, but strongly influence the volume fraction data. Therefore, the volume fraction of precipitates can be taken as the fraction that would have contributed to strength. The volume fraction of

11

precipitates was generally larger for the Ti microalloyed steels compared to the V microalloyed steels. The addition of Mo to the steels increased the volume fraction of precipitates for both Ti- and V-microalloyed steels. For the Mo free steels (N1 and N3) the transformation temperature did not measurably change the volume fraction of precipitates. However, the addition of Mo resulted in a much stronger effect of transformation temperature on volume fraction, particularly for the V microalloyed steel.

Fig. 7 also shows the number density of the precipitates for the 4 steels each at the two transformation temperatures. For all the steels, the number density was lower for transformation at 650°C than 630°C, but the extent of the difference depended on the steel composition. The effect of Mo on the Ti-microalloyed steel was not measurable within statistical error. However, for the V-microalloyed steel, the Mo addition provided a major increase in the precipitate number density for both transformation temperatures.

Fig. 8 shows the precipitate distribution that is characteristic of interphase precipitation. All samples were imaged along <001>, which is the required condition to observe interphase precipitation and also allows all images to be compared. This was the case in all four steels at both isothermal transformation temperatures of 630°C and 650°C for 90min. The average row spacing was greater at the higher isothermal transformation temperature for all steels. Moreover, the row spacing for the Ti-microalloyed steels was smaller than in the V-microalloyed steels. In all Mo containing steels (N2, N4), there were two types of rows, namely rows comprising smaller precipitates (red line) in between rows of larger precipitates (blue line). The rows of finer interphase precipitates in steels N2 and N4, shown in Fig. 8(d, h) were more obvious at the higher isothermal transformation temperature of 650°C. In contrast, for steels N1 and N3, precipitates in between the rows of larger precipitates exhibited a random distribution, Fig. 8(b) and (f) transformed at 650°C.
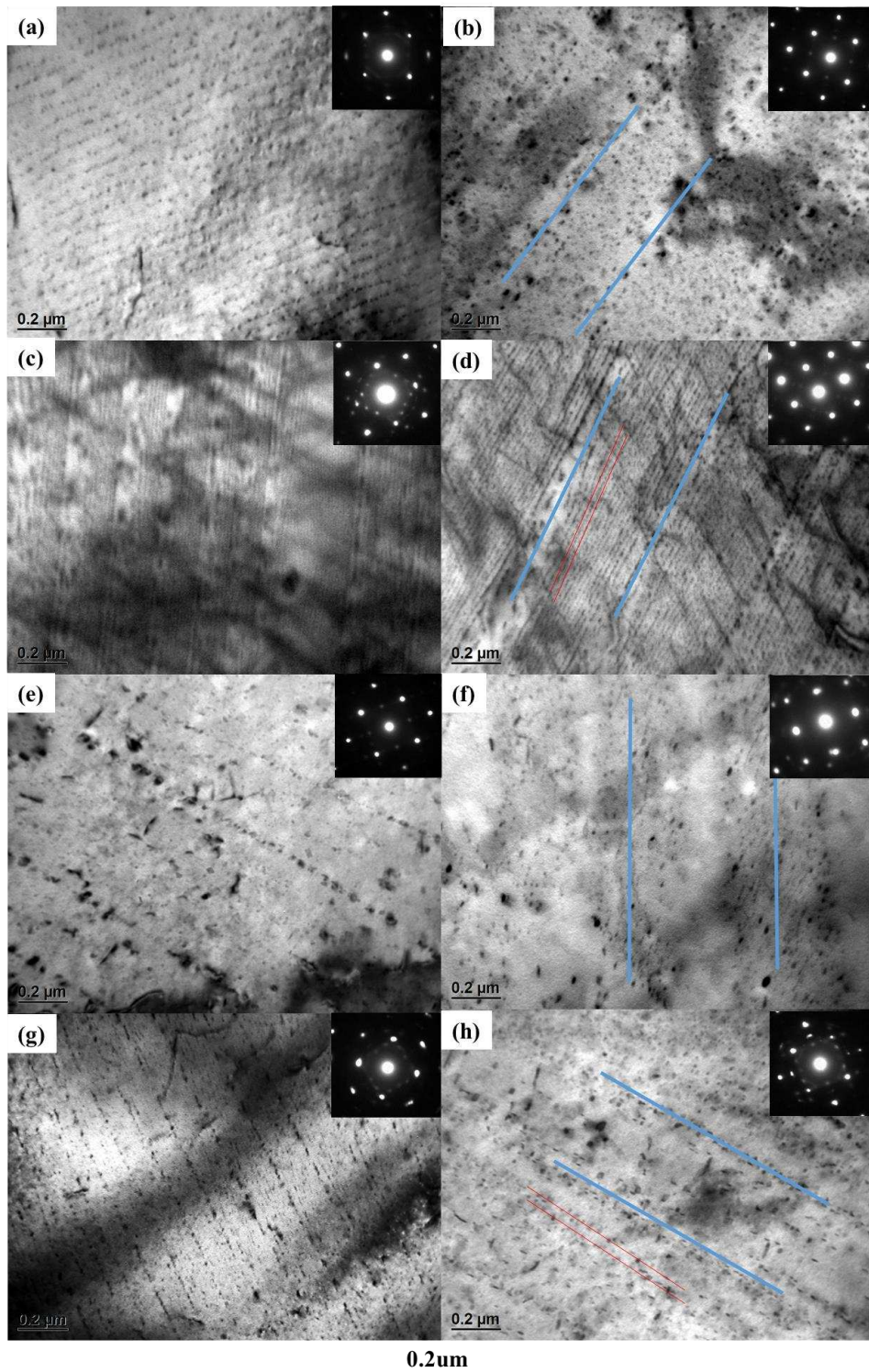
Fig. 8. TEM micrographs showing the interphase precipitation from thin foil samples in different composition of steels taken from isothermal treatment at 630°C for 90min on (a) N1; (c) N2; (e) N3; (g) N4; and at 650°C for 90min on (b) N1; (d) N2; (f) N3; (h) N4.

3.3.2. Precipitate identification and the orientation relationship of interface precipitates with the ferrite

Fig. 9 shows the interphase precipitation rows in more detail for the N2 Ti-Mo microalloyed steel and Fig. 10 gives the equivalent for the N4 Mo-V microalloyed steel, both transformed at 630°C for 90min. The bright field image in Fig. 8(a) was taken with the incident beam parallel to the [001] ferrite zone axis. The diffraction spots from the precipitates are consistent with the presence of both $(Ti,Mo)C$ and $(Ti,Mo)_2C$. The $(Ti,Mo)_2C$ tended to be larger than the $(Ti,Mo)C$. Both exhibited a Baker-Nutting orientation relationship with the ferrite matrix, but with a different variant in each case. The $(Ti,Mo)C$ followed [5]:

$$[100]_{(Ti, Mo)C}//[100]_{ferrite}, \quad (001)_{(Ti, Mo)C}//(001)_{ferrite}$$

and the $(Ti,Mo)_2C$ followed another BN variant[37]:

$$[110]_{(Ti, Mo)2C}//[001]_{ferrite}, \quad (001)_{(Ti, Mo)2C}//(001)_{ferrite}$$

The dark field image shown in Fig. 9(c) was taken from the exactly same area of Fig. 9(a), using diffraction $g(1)=(100)$ and $g(2)=(100)$ (red circle line). The dark field image of Fig. 9(d), shows that the brighter rows of precipitates are from $g(1)$ (yellow line) and the weaker contrast rows of precipitates are from $g(2)$ (red line).
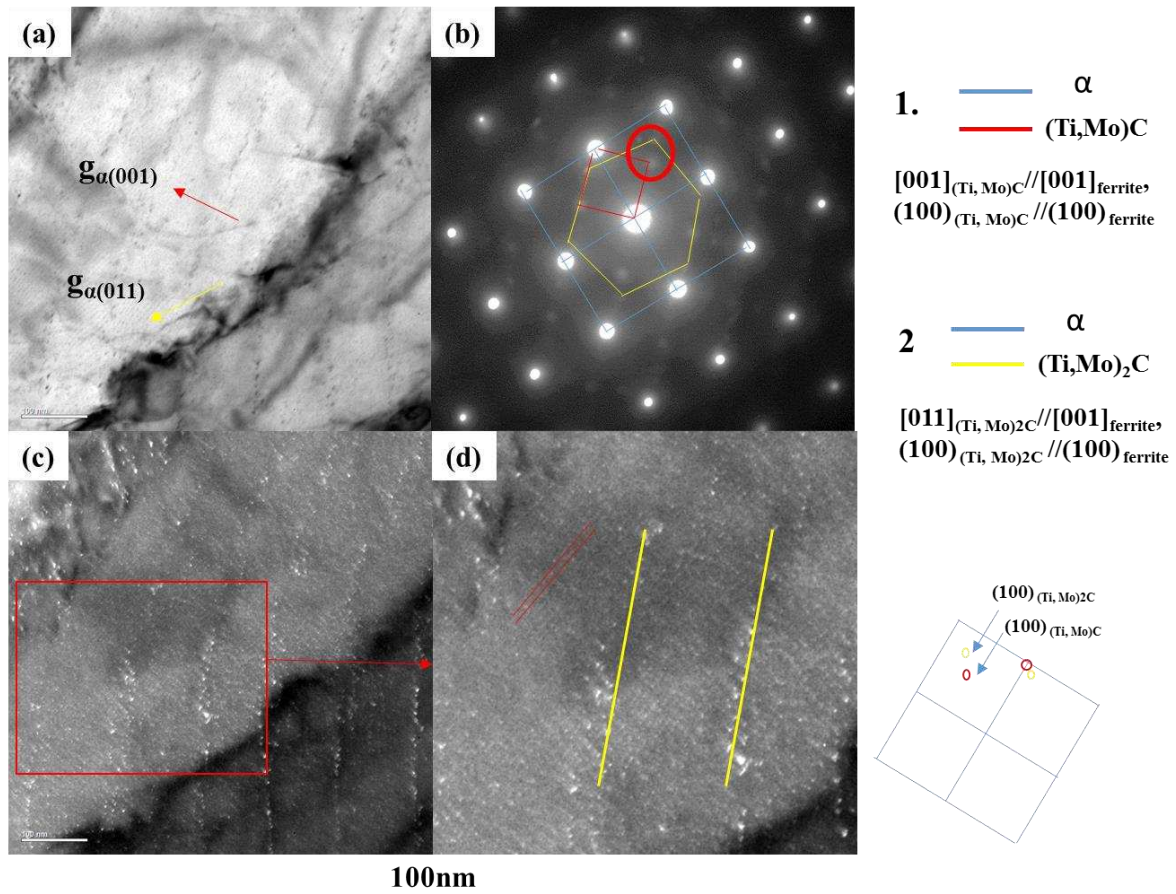
Fig. 9. TEM images of the interphase carbides in the N2 specimens isothermally transformed at 630°C for 90min: (a) bright-field image of interphase precipitation; (b) the corresponding selected area diffraction pattern; (c) dark-field image of interphase precipitation from the red circle in (b) covering the same area of (a); (d) enlarged dark-field image from area indicated by the red line in (c).

Fig. 10 shows bright and dark-field images taken from the V-Mo microalloyed steel, N4. The morphology of the interphase precipitation was similar to the Ti-Mo microalloyed steel in that there were two different orientation relationships with respect to the ferrite matrix. The diffraction patterns were consistent with two precipitate types being present, namely $(V,Mo)C$ and $(V,Mo)_4C_3$. The two orientation relationships were produced by two types of interphase precipitation as shown in Fig. 10(d) with the red line from $(V,Mo)C$ and the yellow line from $(V,Mo)_4C_3$. The corresponding dark-field images shown in Fig. 10(b) from the $(V,Mo)_4C_3$ (yellow circle) and the Fig. 10(c) from $(V,Mo)C$ (red circle). The size of $(V,Mo)_4C_3$ is slightly larger than $(V,Mo)C$.

15
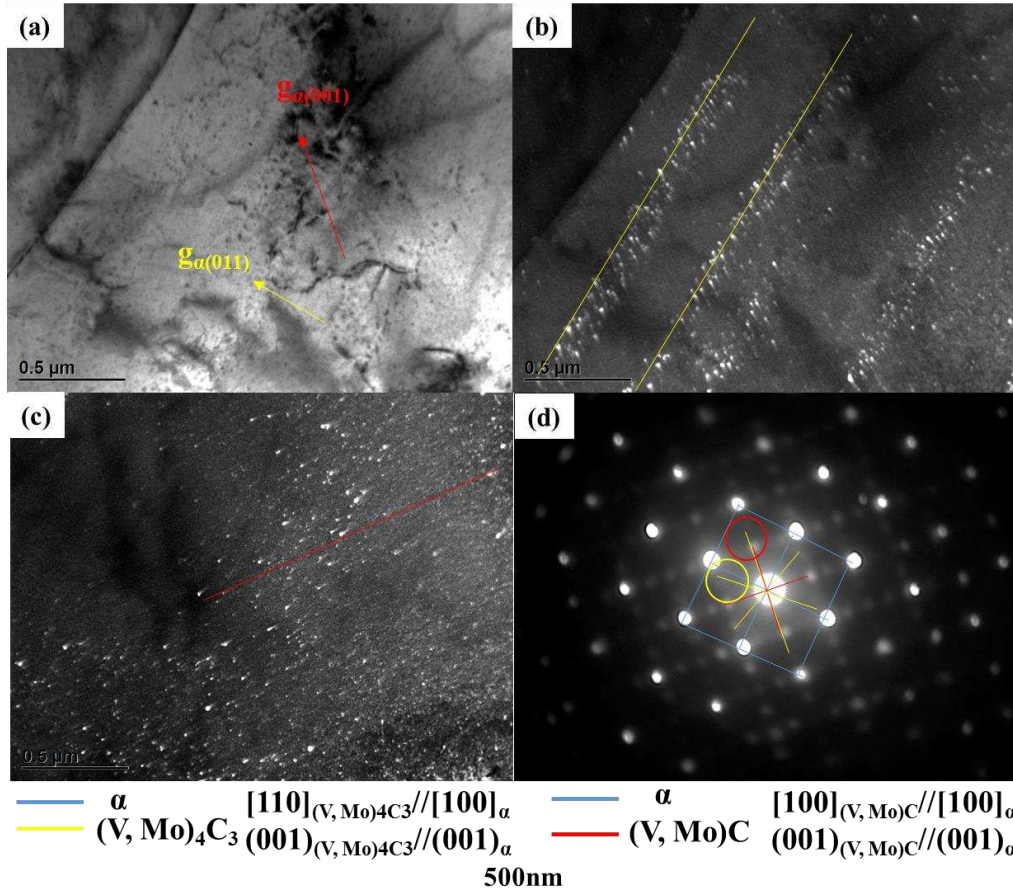
Fig. 10. TEM images of the interphase carbides in the N4 specimens isothermally treated at 630°C for 90min: (a) bright-field image of interphase precipitation; (b) dark-field image of interphase precipitation from the red circle in (d) at the same area of (a); (c) dark-field image of interphase precipitation from the yellow circle in (d) at the same area of (a); (d) the corresponding select area diffraction pattern of (a).

High resolution transmission electron microscopy (HRTEM) images of the precipitates in the ferrite matrix are shown in Fig. 11. The precipitates were coherent with the matrix. The crystal structure and the orientation relationship have been identified by fast Fourier transforms (FFT) of high resolution images shown in Fig. 11(b) and (d). There are two variants of the V based carbides shown in Fig. 11 with the NaCl-type crystal structure. From measurements of the lattice spacing, the ratio $d_{VC\,(200)}/d_{V4C3(200)}$ is equal to 1.031. As reported in [38], the lattice constants for VC is a=b=c=4.165 Å and the V_4C_3 is a=b=c=4.04Å, which gives a ratio $d_{VC(200)}/d_{V4C32(200)}$ of 1.028, which is very close to the measured value. This gives further confirmation that the carbides shown in Fig. 11 are VC in Fig. 11(b) and V_4C_3 in Fig. 11(d).

The (V,Mo)C and (V,Mo)$_4$C$_3$ obeyed the Baker-Nutting (B-N) orientation relationship (OR) with respect to the ferrite matrix:

$$[001]_{(V,Mo)C}//[001]_{ferrite}, \quad (100)_{(V, Mo)C}//(100)_{ferrite}$$

$$[011]_{(V,Mo)4C3}//[001]_{ferrite}, \quad (100)_{(V, Mo)4C3}//(100)_{ferrite}$$

The result is comparable to that for the interphase precipitation in the Ti variant steel, N2 (Fig. 9).
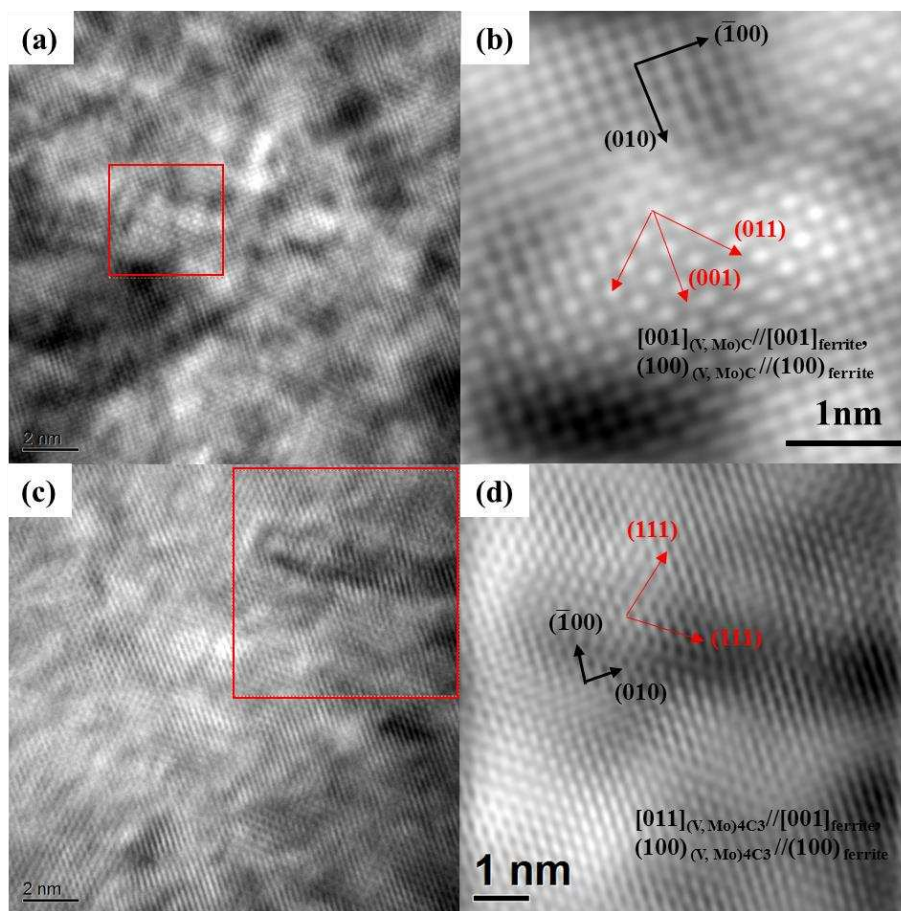
Fig. 11. HRTEM images of nanometer-sized carbides obtained from the specimen isothermally treated at 650°C for 90min: (a) nanometer-sized (V, Mo)C; (b) HRTEM FFT of nanometer sized carbide from red area in (a); (c) nanometer-sized (V, Mo)$_4$C$_3$; (d) HRTEM FFT of nanometer sized carbide from red area in (c).

STEM imaging (Fig. 12) and associated EDS mapping showed that the amount of Mo in the vanadium based carbides varied. The V$_4$C$_3$ appeared to universally contain Mo. However, the finer VC carbides appeared to be separated into two catagories, those containing appreciable Mo and those that contained little or no Mo. This important factor requires further

17

investigation and would need atom probe studies to fully determine composition of the carbides.
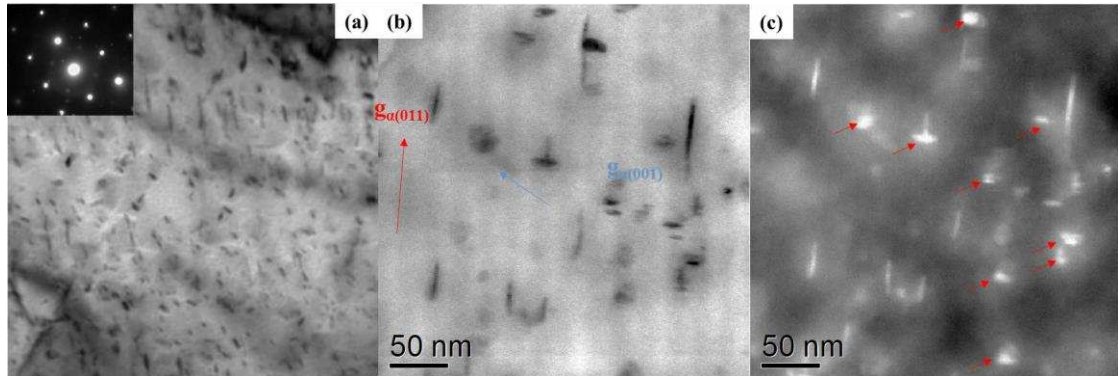
Fig. 12. Two types of precipitates in N4 steel: (a) Bright field STEM image; (b) higher magnification bright field STEM image; (c) corresponding HAADF image from the same area as (b), showing precipitates with differing composition.

3.4 Microhardness

The Vickers microhardness of the ferrite grains is shown in Fig. 13 with isothermal treated at 630°C and 650°C for 90min (martensite grains were excluded from this analysis). From the data points presented in Fig. 13, the microhardness for all four steels decreased with increasing the isothermal transformation temperature. The Ti-microalloyed steels N1 and N2 had higher microhardness for both temperature than that in the V-microalloyed steels. The addition of Mo to N2 and N4 steels resulted in a small increase in the microhardness of the ferrite compared to the Mo free equivalents, N1 and N3.
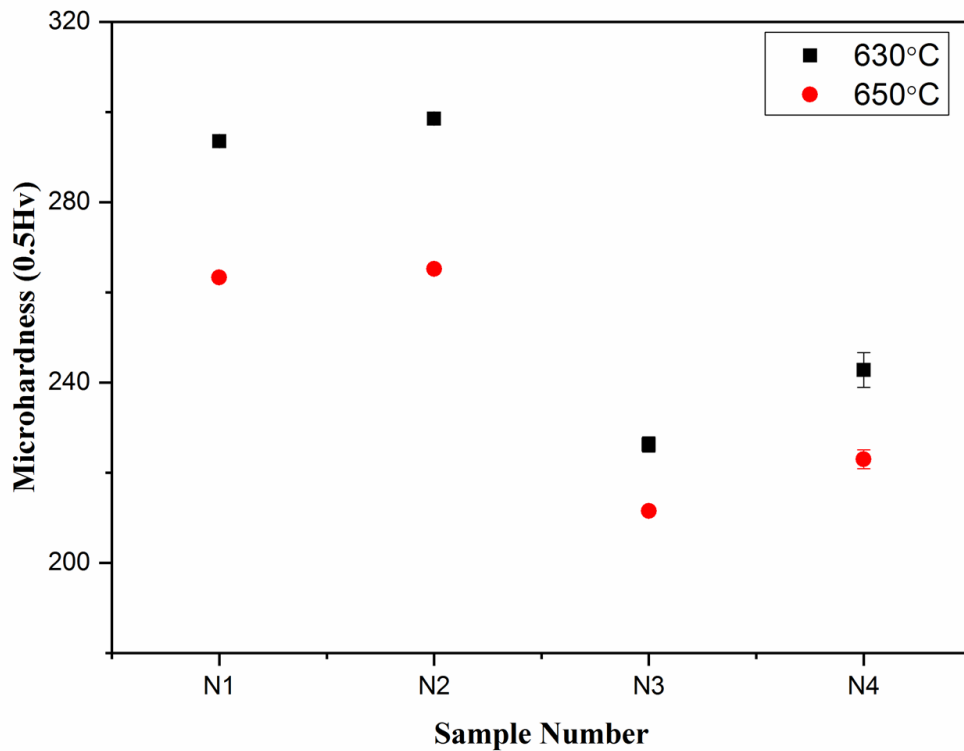
Fig. 13 The Vickers micro hardness of the ferrite grains as a function of the compositions from isothermal treatments at 630°C and 650°C for 90min

4. Discussion

4.1 The mechanism of interphase precipitation

Figs. 5, 6 and 7 gave the morphology, the size distribution, the number density, the volume fraction and the average radius of the precipitates for the steels isothermally transformed at 630°C and 650°C. The formation of carbides on the interface is controlled by the driving force for the carbide nucleation and by the diffusion of carbide-forming elements along the interface. A decrease in the isothermal transformation temperature from 650°C to 630°C increased the nucleation rate due to the increased driving force, resulting in a higher number density of precipitates at the lower transformation temperature. The slower diffusion at the lower temperature also resulted in a finer precipitate size.

19

Fig. 9, 10, 11 also show that the interphase precipitates have the NaCl structure and have the Baker-Nutting OR with ferrite matrix for both Ti and V steels with and without Mo. The addition of Mo did not change the TiC and VC precipitates to the orthorhombic variant.

Fig. 8 shows bright field images from thin foil samples of all four steels. Figs. 9 and 10 give a more detailed analysis from the Ti-Mo steel N2 and V-Mo steel N4. Two different types of precipitate rows were present in N2 and N4, especially for the steels transformed at 650°C. For the Ti bearing steel, the two types of precipitate were $(Ti,Mo)C$ (finer) and $(Ti,Mo)_2C$ (coarser), while for the V bearing steels, $(V,Mo)C$ (finer) and $(V,Mo)_4C_3$ (coarser) were observed. This is, to the best of our knowledge, the first time that two types of precipitate, with different variants of the B-N OR, have been identified within the same area. This was found to be consistent across all the compositions and transformation temperatures investigated.

The morphology of the interphase precipitation was distinctly different for the finer $(Ti,Mo)C$ and the coarser $(Ti,Mo)_2C$ and similarly for the finer $(V,Mo)C$ and the coarser $(V,Mo)_4C_3$. The $(Ti,Mo)C$ and $(V,Mo)C$ formed by classical planer interphase precipitation (PIP) while the $(Ti,Mo)_2C$ and $(V,Mo)_4C_3$ rows, that had a much wider spacing, formed through curved interphase precipitation (CIP). The $(Ti,Mo)_2C$ had a regular sheet spacing and tended to be angled at approximately 45° to the planar precipitate sheets. The dark field images in Fig. 9 were taken under diffraction conditions of $g_{(Ti, Mo)2C}=(100)$ and $g_{(Ti, Mo)C}=(100)$. It is clear that the two types of precipitate had a different orientation with respect to the ferrite matrix, each having one variant of the B-N orientation relationship: the regular CIP (yellow line in Fig. 9) was close to the $(110)_\alpha$ plane, which indicates precipitation on an incoherent austenite/ferrite interface. In contrast, the PIP (red line in Fig. 9) was close to the $(001)_\alpha$ plane with much finer sheet spacing than CIP. The $(V,Mo)_4C_3$ and $(V,Mo)C$, Fig. 10, show the same behaviour

as the (Ti,Mo)C and (Ti,Mo)$_2$C, namely that the (V,Mo)$_4$C$_3$ grew along the (011)$_\alpha$ plane and (V,Mo)C was close to the (100)$_\alpha$ plane.

Where a carbide, such as TiC and VC, is nucleated in the ferrite, all three variants of the B-N orientation relationship are observed [40]. However, where nucleation of the carbide occurs in the γ/α boundary only a single variant is generally found, as was the case here. Thus, the observation of a single variant of the B-N for each precipitate type in the current work strongly suggests that nucleation occurred at the γ/α interface. The observation of a single B-N variant is explained on the basis that where there is a coherent interface between the γ/α, the variant chosen will be the one that makes the close packed planes of all three phases parallel, thereby minimising the free energy for nucleation. In this case, this was identified as the low energy facet plane of (100)$_{(Ti, Mo)C}$//(100)$_\alpha$ and (100)$_{(V, Mo)C}$//(100)$_\alpha$. Thus, the finer (Ti,Mo)C and (V,Mo)C PIP were most probably formed by the classical ledge growth mechanism. In contrast, the coarser (Ti,Mo)$_2$C and (V,Mo)$_4$C$_3$ appeared to have formed by CIP, where the γ/α interface is semi-coherent. In the case of CIP, the precipitates again minimise free energy by aligning one close packed plane as close as possible to the γ/α boundary [38], and therefore one variant of the B-N OR is observed.

The occurrence of CIP and PIP has been shown in different regions of the same grain, for example, by Miyamoto et al. [13], which shows that the interface structure can vary from place to place. Thus, the γ/α interface must have been moving with both semi-coherent and incoherent components at the same time. Yen et al. [15] showed the structure of a ferrite boundary associated with interphase precipitation that contained both ledges and curved regions in between, thus showing that this is possible. However, in their work, only (Ti,Mo)C was identified, rather than how (Ti,Mo)C and (Ti,Mo)$_2$C observed here. Moreover, Miyamoto et al. demonstrated that the transformation front could grow with a coherent region (obeying

the K-S OR), and a less mobile incoherent, non-K-S interface that still exhibited a ledge structure, thus producing interphase precipitation.

The addition of Mo to the Ti and V bearing steels did not alter the orientation relationship observed as shown in Fig. 9, 10 and 11, i.e. the same B-N variant was observed for both TiC and (Ti,Mo)C and similarly for VC and (V,Mo)C.

Fig. 14 gives a schematic to show the formation of coherent PIP interface precipitates in (a), and semi-coherent or incoherent interphase precipitates in (b). It has been well recognized that the newly formed allotriomorphic ferrite nuclei always have rational or nearly rational OR with one of the neighbouring austenite grains, but usually has a random OR with the other adjacent austenite grain [13, 15]. For the PIP, the interface can be composed of an alternating immobile terrace plane and a mobile lateral ledge, i.e. the ledge mechanism. For the semicoherent or incoherent interphase plane the interface is curved and has a high interfacial energy and high mobility. Given that for PIP the ledge structure can be extremely fine in one dimension, precipitation at the ledges leads to the finest precipitate row spacing. In contrast, precipitates formed at a semicoherent or incoherent interface has formed larger precipitates in this case.

(a) Coherent Interphase Plane
$(100)_\gamma$
$(200)_\alpha$
$(200)_{precipitates}$

(b) Semi or Incoherent Interphase Plane
$(111)_\gamma$
$(110)_\alpha$
$(111)_{precipitates}$

γ
α
Precipitates
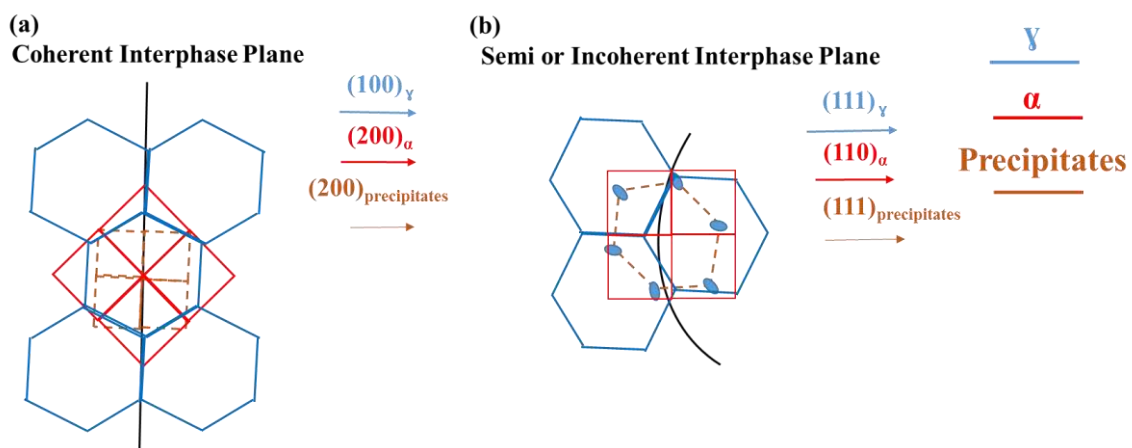
Fig. 14. (a) The schedule of the first type of precipitates with the ledge structure of a partially coherent interface connecting ferrite and austenite by K-S orientation relationship (OR), (b) The structure of the curved semi or incoherent interface connecting ferrite and austenite by random OR.

4.2 The effect of composition on the interphase precipitates

The effect of the Mo on the V-microalloyed steel was much more significant than that on the Ti-microalloyed steel, in particular the addition of Mo reduced the ferrite grain size, reduced the precipitate size significantly and substantially increased the precipitate number density. There are several possibilities for which the Mo can have a major role: the mobility of the γ/α boundary, the chemical free energy of the boundary, the diffusivity along and ahead of the boundary, the interface between precipitate and the matrix and the structure of the precipitate itself.

The nucleation rate can be calculated as [22,40,41]:

$$I = N\frac{kT}{h}\exp\left\{\frac{-(G^*+Q^*)}{kT}\right\} \tag{2}$$

$$G^* = \frac{16\pi}{3}\frac{\sigma^3}{\Delta G_V^2} \tag{3}$$

where N is the number of nucleation sites per unit volume of the system, Q^* is the activation energy for the transfer of atoms across the interface, k is the Boltzmann constant, h is the Planck constant, σ is the interfacial energy per unit area, G^* is the activation energy for nucleation and ΔG_v is the chemical free energy change per unit volume of nuclei. The parameters used in Eqs. (2) and (3) are listed in table 2. This indicates that the sequencing of the nucleation rate for the various carbides is TiC> VC>Mo₂C. Thus, TiC and VC should be nucleated first, with the Mo substituting for the Ti or V in the carbides rather than forming Mo₂C.

The Ti-microalloyed steels exhibited the smallest precipitates of all the steels, which were approximately the same size irrespective of whether Mo was present in the alloy and

irrespective of the transformation temperature, Fig. 7. The absence of a difference in precipitate size between these two transformation temperatures is consistent with the work of Yen et al. [15,42] who found that changes in size only occurred above a transformation temperature of about 680°C. The addition of Mo appears to have slightly increased the number density and volume fraction of precipitates, Figs. 6, 7, which would be consistent with tensile tests that show that the addition of Mo increases the yield strength of the material [43].

Table 2

The equilibrium lattice parameters and formation energy and interfacial energy

type	Chemical free energy /kJ mol^{-1} at 903K [44]	Interfacial energy (σ)/mJ m^{-2}	Diffusion constant (D)/m^2 s^{-1} at 903K
Fe-TiC	-4.2×10^4	339 [45]	1.8×10^{-14} [46]
Fe-VC	-2.2×10^4	199 [8]	3.05×10^{-14} [42]
Fe-Mo$_2$C	-1.3×10^4	256[8]	2.29×10^{-14} [42]

The V-microalloyed steels had a larger precipitates size, a larger ferrite grain size and a greater quantity of martensite compared to the Ti-microalloyed steels. However, the addition of Mo to the V-microalloyed steels reduced the ferrite grain size, reduced the precipitate size significantly and substantially increased the precipitate number density. The inclusion of Mo in TiC or VC results in a contraction of the lattice parameter [8], which results in greater coherency between the precipitate and the matrix. For example, the misfit between TiC and the ferrite is 6.9%, but this is reduced to 4.8% for (Ti,Mo)C [8]. A reduction in interfacial energy will have increased the nucleation rate.

Related work has shown using atom probe tomography that, where Mo is present in the vanadium based carbides, it is evenly distributed throughout the carbide [47]. STEM imaging

(Fig. 12) and EDS mapping showed that Mo was found in all the V_4C_3, aligned approximately along g $=<110>_\alpha$. However, for the VC some precipitates contained Mo, while others did not. Those VC aligned along g$=<100>_\alpha$ contained Mo and so should be referred to as (V,Mo)C. Thus, the two types of precipitate not only had two different orientation relationships with the ferrite, but also had a different composition.

The effect of Mo will also have been through its effect on interfacial velocity and on the row spacing. The row spacing, λ, observed after transformation is related to the interface velocity, $v_{\alpha\gamma}$ through [17]:

$$\lambda = \frac{\pi^{1/4} c_{crit}^{3/2}}{c_p^o b_p^2} \left(\frac{D\sigma_o}{\alpha J_B \Delta G}\right)^{3/4} \left(\frac{3V}{4}\right)^{1/2} \tag{4}$$

$$v_{\alpha\gamma} = \frac{c_{crit}^{1/2} b_p^2}{c_p^o} \left(\frac{D}{\pi}\right)^{1/4} \left(\frac{\alpha J_B \Delta G}{\sigma_o}\right)^{3/4} \left(\frac{4}{3V}\right)^{1/2} \tag{5}$$

Where D is the boundary diffusion of the solute, ΔG is the transformation driving force, J_B is the ferrite nucleation rate, c_{crit} is the critical solute content for carbide precipitation, c_p^o is the nominal solute concentration, b_p is the particle spacing in one row, σ_o is the α/γ interfacial energy and V is the ratio of the molar volume of the precipitate to that of the ferrite. Thus, a reduction in molar volume of the carbide through the inclusion of Mo leads to a reduction in V and therefore an expected reduction in IP row spacing. In addition, Mo would be expected to increase the interfacial energy, σ_o, of the austenite/ferrite transformation boundary, and reduce the solute diffusivity. These factors would decrease the interface velocity, as observed in Fig. 3.

4.3 Strengthening mechanism

Figs. 2 and 3 show the microstructure and the ferrite grain size. The Ti-microalloyed steels exhibited finer ferrite grain size than the V-microalloyed steels for both transformation temperatures. Interestingly, there was a significant difference in ferrite grain size between transformation at 630°C and 650°C for the Ti-microalloyed steel, but relatively little difference for the V-microalloyed steel. The differences in ferrite grain size between the two temperatures cannot be because of the prior austenite grain size as this was the same for a given composition. Therefore, the differences in behaviour between the Ti-microalloyed steel and the V-microalloyed steel must be associated with the balance between the driving force for transformation (which increased as the temperature was decreased) and the diffusion rate (which obviously decreased as the temperature decreased).

Moreover, it is notable that the precipitates formed by PIP were finer than those formed by CIP. It is not clear whether this is inherent to the formation mechanism or whether it is a result of the different precipitate type observed here for the PIP and the CIP. Interestingly, Yen et al. [15] showed that random precipitation occurring from an incoherent interface can give greater hardening than that arising from a coherent boundary leading to classical PIP.

To understand the correlation between grain size, carbide precipitation and strength, the structure-based strength calculation model is used to estimate the strength. The total yield strength was estimated through the friction stress of the ferritic matrix, solid-solute strengthening, grain boundary strengthening and the precipitation strengthening, as well as the dislocation strengthening, which can be expressed as [17,48]:

$$\Delta\sigma total = \Delta\sigma 0 + \Delta\sigma ss + \Delta\sigma GB + \Delta\sigma p + \Delta\sigma s \tag{6}$$

which $\Delta\sigma_{total}$ is the total yield strength; $\Delta\sigma_0$ is the friction stress of single crystal pure iron, $\Delta\sigma_{ss}$ is the solid solution hardening strengthening; $\Delta\sigma_{GB}$ is the grain refinement hardening; $\Delta\sigma_p$ is the precipitation hardening strengthening and $\Delta\sigma_s$ is the dislocation strengthening.

The $\Delta\sigma0$, solid solution hardening strengthening ($\Delta\sigma ss$) and grain refinement strengthening ($\Delta\sigma GB$) according to the composition of the steels in the study can be evaluated by the equation below [28, 29, 31]:

$$\Delta\sigma base = \Delta\sigma 0 + \Delta\sigma ss + \Delta\sigma GB = f^{\frac{1}{3}}\left(35 + 58Mn + 17.4d^{-\frac{1}{2}}\right) + \left(1 - f^{\frac{1}{3}}\right)\left(178 + 3.8s^{-\frac{1}{2}}\right) + 63Si + 426N^{1/2} \qquad (7)$$

Where [%w] (%w =C, Mn, Si, Mn and N) represents the mass fraction of the element %w in ferrite, d is the ferrite grain diameter; f is the volume fraction of ferrite; s is the martensite interlamellar spacing. The mass fractions used for the calculations are list in Table 1.

The interphase precipitation hardening can be given by the Ashby-Orowan relationship [17,19, 49]:

$$\Delta\sigma p = 8995 * \frac{f^{\frac{1}{2}}}{d_p}\ln(2.417d_p) \qquad (8)$$

where f is the volume fraction of the interphase precipitation, d_p is the average diameter of precipitation (nm), which are shown in Fig. 7 in this study.

This analysis did not differentiate between the contribution from the different precipitate types. It is difficult to separate the contribution to hardening of the rod shaped $(V,Mo)_4C_3$ (which grew along the $(011)_\alpha$ plane) from the disc shaped (V,Mo)C (which grew along the $(100)_\alpha$ plane) and equally the contribution of the (Ti,Mo)C from the $(Ti,Mo)_2C$. The $(V,Mo)_4C_3$ and the $(Ti,Mo)_2C$ exhibited a much lower volume fraction and were coarser than the (V,Mo)C and (Ti,Mo)C respectively, as so would have contributed only minor part to the hardening. Therefore the majority of hardening would have come from the (V,Mo)C and (Ti,Mo)C.

The increased yield stress resulting from the increased dislocation density can be estimated by [30]:

$$\Delta\sigma s = \alpha M G b \sqrt{\rho} \qquad (9)$$

Where α is a constant of 0.435; M is the Taylor factor and for ferrite steel, it equal to 2.75; G is the shear modulus, taken as 80.3 GPa; b is the Burgers vector (0.248nm); ρ is the dislocation density. The dislocation density in the ferrite matrix during isothermal transformation is estimated to be 5×10^{13} m^{-2}.

Therefore, the total yield stress can be estimated by Eqs. (6)-(10) and the results are presented in Fig. 15. The contribution of interphase precipitation was estimated as around 127-236MPa, with the highest value observed for N2. The Ti containing steels exhibited the finest ferrite grain size and therefore the greatest Hall Petch strengthening. When Mo is added to both Ti-microalloyed and V-microalloyed steels, the volume fraction of interphase precipitates increased, with a much more significant effect in the V-microalloyed steels than Ti-microalloyed steels.
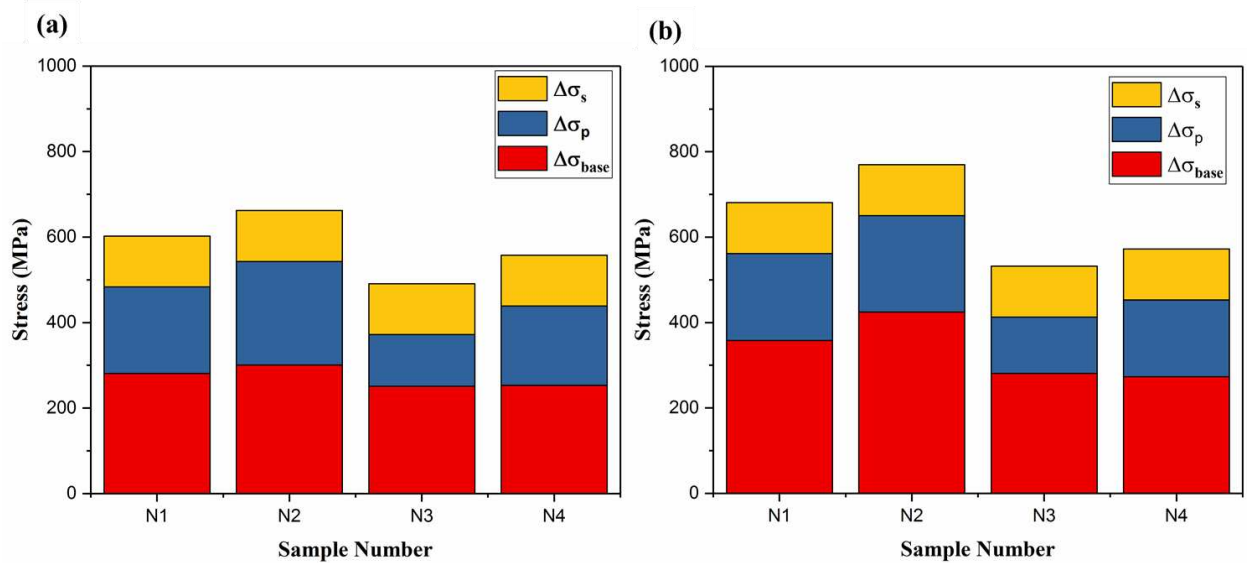
The microhardness for all four steels were measured and shown in Fig. 13. The relation between yield strength and hardness has been determined to be [49]:

$$YS = -90.7 + 2.876Hv \tag{10}$$

where yield strength has units of MPa and Hv is diamond pyramid hardness which uses traditional units (kgf/mm^2). Therefore, the yield strengthen according to the microhardness could be estimated and shown in Fig. 16. The general trend of the composition dependence for the calculated yield strength by Eqs. (6)-(9) is consistent with that from Eq. (10) depending on the measurements of Vickers hardness. Therefore, the calculated yield strength with the Eqs. (6)-(9) are consistent with the measurement of the ferrite grain size, the volume fraction and the size of the precipitates from all four steels.
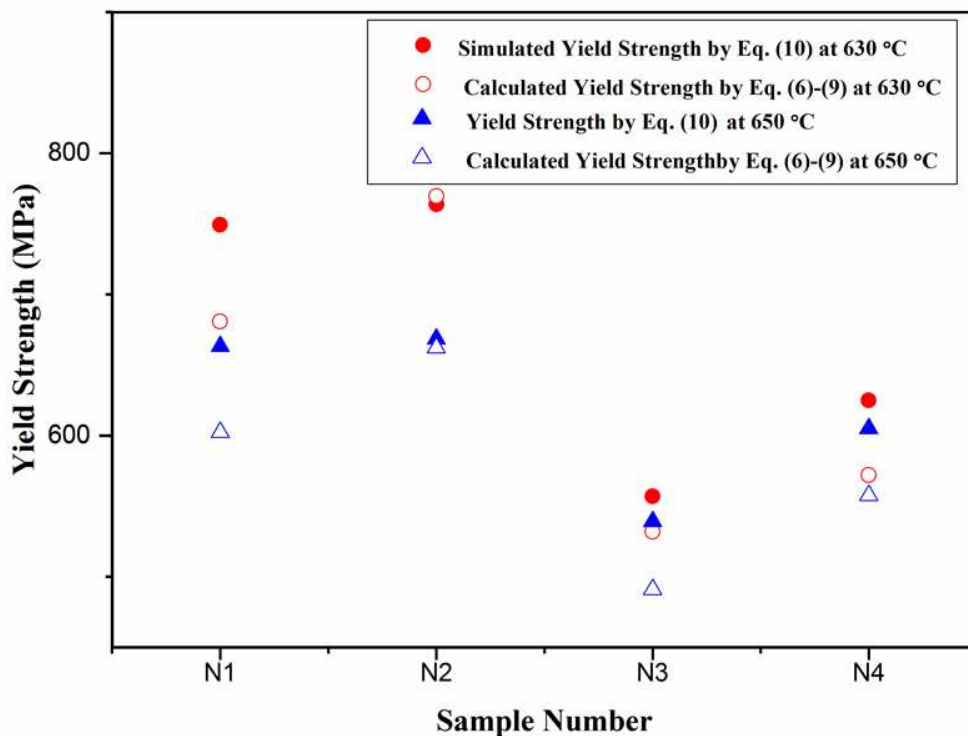

Fig. 16. Simulated yield strength from Eq. (6)-(9) with isothermally treated at 630°C and 650°C for 90min, compared with yield strength estimated from the micro hardness by Eq. (10).

5. Conclusions

The interphase precipitation in Ti-microalloyed and V-microalloyed steels with and without Mo additions, but with otherwise identical composition, was studied after isothermal transformation at 630°C and 650°C for 90min with the following conclusions:

1) The ferrite grain size in the Ti-microalloyed steels was smaller than in the V-microalloyed steels at both isothermal transformation temperatures of 630°C and 650°C for 90min. The number density of the precipitates in the Ti-microalloyed steels was higher than that in the V-microalloyed steels, and the average precipitate size was significantly smaller for the same transformation conditions. For both Ti and V microalloyed steels all microstructural features were coarser following transformation at 650°C compared to 630°C.

2) There were two types of the interphase precipitates in all steel compositions and transformation conditions. For the Ti bearing steel, TiC (finer) and Ti_2C (coarser) were observed in the same areas of the sample, while for the V bearing steels, VC (finer) and V_4C_3 (coarser) were observed, again in the same area of the sample. Where Mo was present in the alloy, it was found dissolved in all carbide types. The (Ti,Mo)C and (V,Mo)C formed by classical planer interphase precipitation (PIP) while the $(Ti,Mo)_2C$ and $(V,Mo)_4C_3$ rows, which had a much wider spacing, formed through curved interphase precipitation (CIP). Each adopted one variant of the Baker-Nutting orientation relationship.

3) The addition of Mo to the Ti bearing steel was found to reduce the transformation kinetics which resulted in a higher volume fraction of precipitates, but did not significantly alter the precipitate size. For the V bearing steel, the addition of Mo significantly reduced the austenite to ferrite transformation kinetics. The effect of the Mo on the V-microalloyed steel was much more significant than that on the Ti-

30

microalloyed steel, in particular the addition of Mo reduced the ferrite grain size, reduced the precipitate size significantly and substantially increased the precipitate number density and volume fraction. The Mo was believed to reduce the misfit between the V based carbide and the matrix, reducing interfacial energy and allowing a much greater nucleation density.

4) The contribution of the fine precipitates and the grain size to the yield strength was estimated. There was generally good agreement between calculated strengths and those estimated through microhardness. The interphase precipitation in the ferrite resulted in a maximum contribution to strength of around 127-236MPa in the four alloy steels.

Acknowledgements

References

[1]   M. Mannerkoski, On the kinetics of precipitate dissolution, Met. Sci. J. 3 (1969) 95-97.

[2]   K. Relander, Austenitzerfall eines 0.18%C-2%Mo-Stahles im Temperaturbereich der Perlitstufe, Acta Polytech. Scand. Incl. Metall. Ser. 26 (1964) 34.

[3]   J. V Wood, R.W.K. Honeycombe, Splat queching of austenitic steels, Mater. Sci. Eng. 23 (1976) 107-112.

[4]   R.A. Ricks, P. R. Howell, G. S. Barritte, The nature of acicular ferrite in HSLA steel weld metals, J Mater. Sci. 17 (3) (1982) 732-740.

[5]   M.Y. Chen, H.W. Yen, J.R. Yang, The transition from interphase-precipitated carbides to fibrous carbides in a vanadium-containing medium-carbon steel, Scr. Mater. 68 (2013) 829-832.

[6]   R.W.K. Honeycombe, 29th hafield memorial lecture: ferrite, Met. Sci. 14 (2013) 201-214.

[7]   R.A. Ricks, P.R. Howell, The formation of discrete precipitate dispersions on mobile interphase boundaries in iron-base alloys, Acta Mater. 31 (6) (1983) 853-861.

[8]   J. Jang, C. Lee, Y. Heo, D. Suh, Stability of (Ti, M) C (M= Nb, V, Mo and W) carbide in steels using first-principles calculations, Acta Mater. 60 (2012) 208-217.

[9]   F.A. Khalid, D.V. Edmonds, Interphase precipitation in microalloyed engineering steels and model alloy, Mater. Sci. Tech. 9 (1993) 384-396.

[10]   H. Najafi, J. Rassizadehghani, S. Asgari, As-cast mechanical properties of vanadium/niobium microalloyed steels, Mater. Sci. Eng. A. 486 (2008) 1-7.

[11]   H.K.D.H. Bhadeshia, The lower bainite transformation and the significance of carbide precipitation, Acta Mater. 28 (1980) 1103-1114.

[12]   Q. Liu, W. Liu, X. Xiong, Correlation of Cu precipitation with austenite–ferrite transformation in a continuously cooled multicomponent steel: An atom probe tomography study, J. Mater. Res. 27 (2012) 1060-1067.

[13]   G. Miyamoto, R. Hori, B. Poorganji, T. Furuhara, Crystallographic Analysis of Proeutectoid Ferrite/Austenite Interface and Interphase Precipitation of Vanadium Carbide in Medium-Carbon Steel, Metall. Mater. Trans. A. 44 (2013) 3436-3443.

[14]   A. T. Davenport, F. G. Berry, R.W. K. Honeycombe, Interphase Precipitation in Iron Alloys, Met. Sci. J. 2 (2013) 104-106.

[15]   H.W. Yen, P.Y. Chen, C.Y. Huang, J.R. Yang, Interphase precipitation of nanometer-sized carbides in a titanium–molybdenum-bearing low-carbon steel, Acta Mater. 59 (2011) 6264-6274.

[16]   A. Karmakar, S. Kundu, S. Roy, S, Neogy, D. Srivastava, D. Chakrabarti, Effect of microalloying elements on austenite grain growth in Nb-Ti and Nb-V steels, Mater. Sci. Tech. 30 (2014) 653-664.

[17]   M.Y. Chen, M. Gouné, M. Verdier, Y. Bréchet, J. R. Yang, Interphase precipitation in vanadium-alloyed steels: Strengthening contribution and morphological variability with austenite to ferrite transformation, Acta Mater. 64 (2014) 78-92.

[18]   J. Hu, L.X. Du, J.J. Wang, C.R. Gao, T.Z. Yang, A.Y. Wang, R.D.K. Misra, Microstructures and Mechanical Properties of a New As-Hot-Rolled High-Strength DP Steel Subjected to Different Cooling Schedules, Metall. Mater. Trans. A. 44 (2013) 4937-4947.

[19]   H.J. Kestenbach, S.S. Campos, E.V. Morales, Role of interphase precipitation in microalloyed hot strip steels, Mater. Sci. Technol. 22 (2013) 615-626.

[20]   G. Purdy, The dynamics of transformation interfaces in steels-I. The ferrite-austenite interface in Fe-C-Mo alloys, Acta Metall. 26 (1978) 477-486.

[21] N.K. Balliger, R.W. K. Honeycombe, The effect of nitrogen on precipitation and transformation kinetics in vanadium steels, Metall. Trans. A. 11 (1980) 421-429.

[22] M. Hillert, G.R. Purdy, Chemically induced grain boundary migration, Acta Metall. 26 (1978) 333-340.

[23] J.A. Todd, P. Li, Microstructure-mechanical property relationships in isothermally transformed vanadium steels, Metall. Trans. A. 17 (1986) 1191-1202.

[24] A.D. Batte, R.W. K. Honeycombe, Precipitaion of vanadium carbide in ferrite, J. Iron Steel Inst. 211 (1973) 284-289.

[25] R. Lagneborg, T. Siwecki, S. Zajac, B. Hutchinson, The Role of vanadium in microalloyed steels, Scand. J. Metall. 28 (1999) 186-241.

[26] R.A. Ricks, P.R. Howell, R.W.K. Honeycombe, Formation of supersaturated ferrite during decomposition of austenite in iron–copper and iron-copper-nickel alloys, Met. Sci. 14 (2013) 562-568.

[27] T. Sakuma, R.W. K. Honeycombe, Effect of manganese on microstructure of an isothermally transformed Fe–Nb–C alloy, Mater. Sci. Technol. 1 (2013) 351-356.

[28] V.B. Ginzburg, Steel-Rolling technology: theory and practice, CRC Press New York, 1989.

[29] K. Zhang, Z.D. Li, X. J. Sun, Q. L. Yong, J. W. Yang, Y. M. Li, P. L. Zhao, Development of Ti-V-Mo Complex Microalloyed Hot-Rolled 900-MPa-Grade High-Strength Steel, Acta Metall. Sin. 28 (2015) 641-648.

[30] N. Kamikawa, Y. Abe, G. Miyamoto, Y. Funakawa, Tensile Behavior of Ti , Mo-added Low Carbon Steels with Interphase Precipitation, ISIJ Int. 54 (2014) 212-221.

[31] Y.W. Kim, S.W. Song, S.J. Seo, S.G. Hong, C.S. Lee, Development of Ti and Mo micro-alloyed hot-rolled high strength sheet steel by controlling thermomechanical controlled processing schedule, Mater. Sci. Eng. A. 565 (2013) 430-438.

[32] M.G. Akben, P. Plassiard, J.J. Jonas, Dynamic precipitation and solute hardening in a titanium microalloyed steel containing three levels of manganese, Acta Metall. 32 (1984) 591-601.

[33] M.S. EI-Genk, J.M. Tournier, A review of refractory metal alloys and mechanically alloyed-oxide dispersion strengthened steels for space nuclear power systems, J Nucl. Mater. 340 (2005) 93-112.

[34] M. Aghaie-Khafri, F. Fazlalipour, Kinetics of V(N,C) coating produced by a duplex surface treatment, Surf. Coatings Technol. 202 (2008) 4107-4113.

[35] D. C. Joy, R. F. Egerton, D. M. Maher, Progress in the quantitation of electron energy-loss spectra, Scanning Electron Microsc. 124 (1979) 817-826.

[36] R. Leapman, Detecting single atoms of calcium and iron in biological structures by electron energy-loss spectrum-imaging, J. Microsc. 210 (2003) 5-15.

[37] M.A. Altuna, B. Pereda, I. Gutie, M. Society, Precipitation of Nb in Ferrite After Austenite Conditioning . Part I : Microstructural Characterization, Metall. Mater. Tran. A 43 (2012) 4553-4570.

[38] X. Chong, Y. Jiang, J. Feng, RSC Advances Electronic structures mechanical and thermal properties of V-C binary compounds, RSC Adv. 4 (2014) 44959-44971.

[39] R.M. Smith, D.P. Dunne, Structural aspects of alloy carbonitride precipitation in microalloyed steels, Mater. Forum. 11 (1988) 166-181.

[40] R. Lagneborg, S. Zajac, A model for interphase precipitation in V-microalloyed structural steels, Metall. Mater. Trans. A. 32 (2001) 1-12.

[41] S. Yamasaki, H. K. D. H. Bhadeshia, M_4C_3 precipitation in Fe–C–Mo–V steels and relationship to hydrogen trapping, Proc. R. Soc. A Math. Phys. Eng. Sci. 462 (2006) 2315-2330.

[42] H.W. Yen, C.Y. Huang, J.R. Yang, Characterization of interphase-precipitated nanometer-sized carbides in a Ti-Mo-bearing steel, Scr. Mater. 61 (2009) 616-619.

[43] A. Fatehi, J. Calvo, A. M. Elwazri, S. Yue, Strengthening of HSLA steels by cool deformation, Mater. Sci. Eng. A. 527 (2010) 4233-4240.

[44] S. Shatynski, The thermochemistry of transition metal carbides, Oxid. Met. 13 (1979) 105-118.

[45] A. Teresiak, H. Kubsch, X-ray investigations of high energy ball milled transition metal carbides, Nanostructured Mater. 6 (1995) 671-674.

[46] H. W. Hugosson, P. Korzhavyi, U. Jansson, B. Johansson, O. Eriksson, Phase stabilities and structural relaxations in substoichiometric TiC_{1-x}, Phys. Rev. B. 63 (2001) 165116.

[47] Y-S. Chen, D. Haley, S.S.A. Gerstl, A.J. London, F. Sweeney, R.A. Wepf, W.M. Rainforth, P.A.J. Bagot, M.P. Moody, Direct observation of individual hydrogen atoms at trapping sites in a ferritic steel, Science **355**(6330) 1196-1199.

[48] N. KAMIKAWA, Y. ABE, G. MIYAMOTO, Y. FUNAKAWA, T. FURUHARA, Tensile behavior of Ti, Mo-added low carbon steels with interphase precipitation, ISIJ international 54 (2014) 212-221.

[49] S. C. Krishna, N. K. Gangwar, A. K. Jha, B. Pant, On the Prediction of Strength from Hardness for Copper Alloys, J. Mater. 2013 (2013) 1-6.